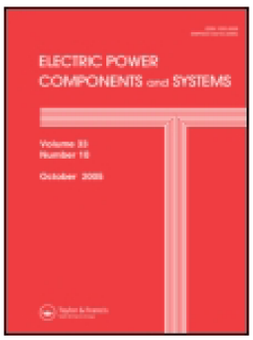

Taylor & Francis
Taylor & Francis Group

Electric Power Components and Systems

ISSN: 1532-5008 (Print) 1532-5016 (Online) Journal homepage: http://www.tandfonline.com/loi/uemp20

Modeling and Affine Parameterization for Dual Active Bridge DC-DC Converters

Imran Syed, Weidong Xiao & Peng Zhang

To cite this article: Imran Syed, Weidong Xiao & Peng Zhang (2015) Modeling and Affine Parameterization for Dual Active Bridge DC-DC Converters, Electric Power Components and Systems, 43:6, 665-673, DOI: 10.1080/15325008.2014.997327

To link to this article: https://doi.org/10.1080/15325008.2014.997327

Electric Power Components and Systems, 43(6):665–673, 2015

ISSN: 1532-5008 print / 1532-5016 online
DOI: 10.1080/15325008.2014.997327

Taylor & Francis
Taylor & Francis Group

Modeling and Affine Parameterization for Dual Active Bridge DC-DC Converters

Imran Syed,[1] Weidong Xiao,[1] and Peng Zhang[2]
[1]Electrical Engineering & Computer Science, Masdar Institute of Science & Technology, Abu Dhabi, UAE
[2]Department of Electrical and Computer Engineering, University of Connecticut, Storrs, Connecticut, USA

CONTENTS

Abstract—This article proposes a dynamic modeling and control approach for dual active bridge converters, which have attracted significant attention for its merits of bi-directional power flow and soft switching capability. Due to the non-linear nature of dual active bridges, the techniques of averaging and linearization are utilized to derive the small-signal model. The affine parameterization is then presented for designing the closed-loop system to regulate the output voltage. The effectiveness of the modeling process and closed-loop regulation is verified by experimental evaluation.

1. INTRODUCTION

With the rapid rise of battery-operated electric vehicles, DC-output renewable resources, solid state transformers, and DC distributed power systems, the topology of dual active bridge (DAB) converters draws significant attention and shows the advantages of bi-directional power flow capability, high power density, power controllability, high power capability, buck/boost operation, and inherent soft switching [1]–[5]. Figure 1 shows the schematic of a conventional DAB converter comprising two bridges (B_1 and B_2) that are interconnected through high-frequency transformer T_r. The phase shift between B_1 and B_2 creates the voltage difference between V_{T1} and V_{T2}/N, determines the magnitude of the current flowing through inductor Ls, and eventually controls the power flow in both directions between the left and right terminals. Both bridges adopt the same switching frequency and a constant 50% duty cycle; therefore, the degree of phase shift is the only control variable for regulating the average active power delivery.

Significant research effort mainly focuses on efficiency improvement by ways of minimizing circulation current or reactive power components [6] and extending soft-switching ranges [2-7]. The loss model was presented in [8], and several improved modulation techniques were proposed in [5][6], [9]-[12]. The characteristics of DAB operation were analyzed and presented in [13], which led to a direct single-loop voltage

Keywords: DC/DC converter, dual active bridge, modeling, digital control, affine parameterization
Received 9 April 2014; accepted 30 November 2014
Address correspondence to Prof. Peng Zhang, Department of Electrical and Computer Engineering, University of Connecticut, 371 Fairfield Way, U-4157, Storrs, CT 06269-4157, USA. E-mail: peng@engr.uconn.edu
Color versions of one or more of the figures in the article can be found online at www.tandfonline.com/uemp.

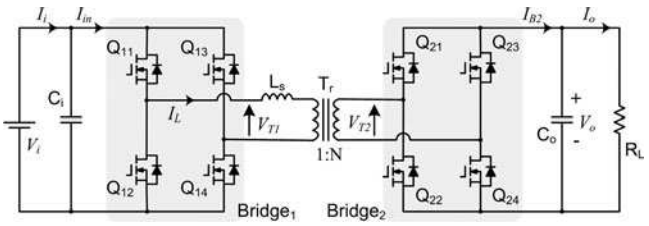

FIGURE 1. Schematics of DAB converter.

control strategy. One study focused on the bidirectional feature of the DAB and proposes a control scheme to use the high-frequency AC-link current of the DAB DC-DC converter as a control variable [14] to improve dynamic performance. However, the above techniques do not reveal the linear modeling approach, which is widely utilized for synthesizing controllers.

Since dynamic analysis and feedback control play a critical role in real-world power electronic applications, it is important to find an effective way to characterize DAB dynamics, synthesize controllers, and adopt proper control strategies that guarantee system stability and support the goal of high efficiency and power density. In the DAB, the control objective includes the following: (a) output voltage regulation for standalone power supply systems [15][16]; (b) input voltage regulations for photovoltaic power interfaces [17]; and (c) hybrid regulation of voltage and current for battery management in electric vehicles [11], bi-directional control operation [14], [18], and load sharing control for DC distributed power systems [18]. A harmonic modeling approach was proposed in [15] using the Fourier series to identify the system dynamics accurately. The study in [19] presents an integrated control algorithm to balance both the rectifier capacitor voltage and active power distribution among parallel DAB modules. The controller synthesis is based on a single-phase *dq* model to best fit the specific application. One modeling approach was presented in [20] using the switching frequency terms in the Fourier series of state variables and high-order state-space models, aiming to capture the effects of purely AC transformer current on converter dynamics. The studies in [21-22] focused on the modeling accuracy for digital control implementation and developed a small-signal model based on the state-space and discrete-time representation. However, the above modeling techniques are generally complicated for power electronic engineers to adopt and use effectively for controller synthesis. In [16], the DAB dynamics were treated as a non-linear problem; therefore, the Lyapunov stability criterion is used for DAB stability analysis. A non-linear control strategy for DAB was proposed in [23].

Since linear control techniques, *i.e.*, the proportional-integral-derivative (PID) type, are dominantly used in power electronic systems, the non-linear system approach is not a practical way to analyze DAB dynamics and provide an effective control solution. Another modeling approach was presented in [24] that utilized state-space averaging techniques. The inductor current was selected to represent one of the state variables. Due to the AC characteristics of the inductor current, that work demonstrated a very complex derivation for the averaging process. It turns out to provide the same modeling result as the simplified modeling approach introduced in [25]. Although the model effectiveness was proved by simulation in [25], the dynamic analysis focuses on a specific operating point and does not cover variation of operating conditions, including the change of phase shift, buck or boost operating mode, and loads. How to integrate the presented model with the controller design is also unclear in the prior study.

Due to the complexity of non-linear control techniques, this study mainly focuses on model linearization and linear control approaches that are widely utilized in controlling power converters. It is desirable to develop a simple and effective DAB model that represents the practical system. The key dynamic characteristics of DAB converters should be revealed in depth for effective control analysis and design. Therefore, this article presents a general approach for modeling and control of DAB converters and is organized as follows. Section 2 describes the modeling approach for DAB converters. The dynamic characteristics are discussed in detail in corresponding to the change of loads and operating conditions. Based on the derived model, the control synthesis is presented in Section 3. The affine parameterization is used to ensure the robustness and stability of the closed-loop system. Section 4 shows the simulation and experimental evaluation, where the proposed model is verified by both simulation and experimental results covering the variation of operating conditions. The closed-loop control performance is experimentally demonstrated to show the effectiveness of the presented control study. The evaluation demonstrates the performance of effective load disturbance rejection and good command following.

2. DYNAMIC MODELING AND CONTROL

Figure 2 illustrates the waveforms of voltage and current when the DAB is operated at steady state. δ indicates the phase shift between the two bridges, B_1 and B_2. The power flow equation was derived in [26], and a general form can be expressed as

$$P_o = \frac{V_{in} V_2 \delta(\pi - \delta)}{\omega L_s \pi N}. \quad (1)$$

V_{in}, V_2, and L_s refer to the diagram in Figure 1. ω is the radian representation of switching frequency. The operating mode shown in Figure 2 is called the buck operation since

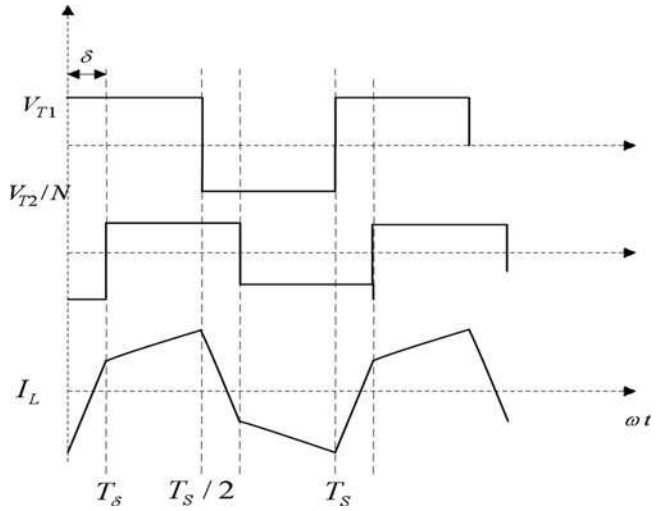

FIGURE 2. Typical voltage and current waveforms in steady state of DAB.

the value of $|V_{T1}|$ is higher than that of $|V_{T2}|$/N. Another two operating modes are defined as boost and flat-top [2].

2.1. Output Voltage Dynamics

Inductance L_s is relatively small in value since it responds to the high-frequency switching and forms an impedance effect to limit the power flow magnitude. The high-frequency dynamics of the inductor are neglected at the beginning because the dominant frequency results from the low-frequency components in dynamic systems. Therefore, concentration is on the dynamics of output filter C_2 and load R_L, and the two-bridge converter is treated as a variable power source:

$$C_2\frac{dv_2(t)}{dt} = \frac{P_o}{V_2} - \frac{v_2(t)}{R_L}, \tag{2}$$

where $v_2(t)$ is the variable representation of output voltage V_2 in a steady-state condition; for other symbols, refer to Figure 1.

Parameters	Change	Magnitude K_0	Time constant τ_0
Operational parameters	R_L increasing	Increasing	Increasing
Design parameters	δ increasing	Decreasing	No effect
	C_2 increasing	Non effect	Increasing
	f_s increasing	Decreasing	No effect
	L_s increasing	Decreasing	No effect
	N increasing	Decreasing	No effect

TABLE 1. Parameter effect on plant dynamics

System parameters	Values
Input voltage, V_{in}	30 V
Output voltage, V_2	150 V
Switching frequency, f_s	200 kHz
Inductance, L_s	2.2 μH
Output capacitance, C_2	500 μF
Nominal load resistance, R_L	132.5 Ω
Transformer turn, N	6
Converter peak efficiency	91%

TABLE 2. System parameters

Following Eqs. (1) and (2) gives

$$C_2\frac{dv_2(t)}{dt} = \frac{V_{in}\delta(t)[\pi - \delta(t)]}{\omega L_s \pi N} - \frac{v_2(t)}{R_L}, \tag{3}$$

Non-linearity is shown in Eq. (3) since both $v_2(t)$ and $\delta(t)$ are time variants. A linearization process shown in Eq. (4) is needed to derive the small-signal equation, as shown in Eq. (5):

$$C_2\frac{d\tilde{v}_2}{dt} = \left.\frac{\partial f}{\partial \delta}\right|_{\delta, V_2}\tilde{\delta} + \left.\frac{\partial f}{\partial v_2}\right|_{\delta, V_2}\tilde{v}_2, \tag{4}$$

$$C_2\frac{d\tilde{v}_2(t)}{dt} = \frac{V_{in}}{N\omega L_s}\left(1 - \frac{2\delta}{\pi}\right)\tilde{\delta}(t) - \frac{1}{R_L}\tilde{v}_2(t). \tag{5}$$

Symbols of $\tilde{\delta}(t)$ and $\tilde{v}_2(t)$ stand for the small-signal time variants of phase shift and output voltage, respectively, from a certain operating point, which is determined by the steady-state value of phase shift δ. The dynamic equation can finally be transformed to the s-domain transfer function, as shown in Eqs. (6) or (7):

$$\frac{\tilde{v}_2(s)}{\tilde{\delta}(s)} = \frac{\frac{V_{in}R_L}{2\pi f_s L_s N}\left(1 - \frac{2\delta}{\pi}\right)}{R_L C_2 s + 1}, \tag{6}$$

$$G_0(s) = \frac{K_0}{\tau_0 s + 1}, \tag{7}$$

δ	R_L (Ω)	P_o (W)	G_0
16°	350.0	64.3	$\frac{517.5}{0.175s+1}$
20°	300.0	75.0	$\frac{424.9}{0.15s+1}$
24°	250.0	90.0	$\frac{331.0}{0.125s+1}$
32°	200.0	112.5	$\frac{234.4}{0.1s+1}$
58°	132.5	170.0	$\frac{84.45}{6.63e^{-2}s+1}$

TABLE 3. Plant transfer functions based on operating conditions.

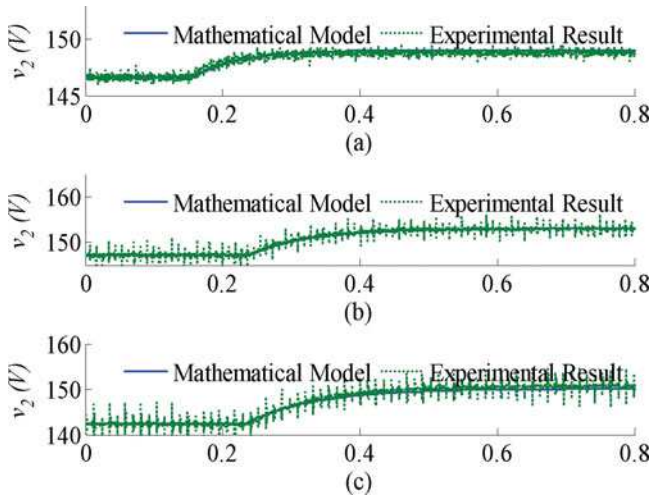

FIGURE 3. Step response comparison of the output voltage between the mathematical model and experimental results based on four steady-state conditions: (a) 132.5-ohms load, (b) 175-ohms load, (c) 200-ohms load.

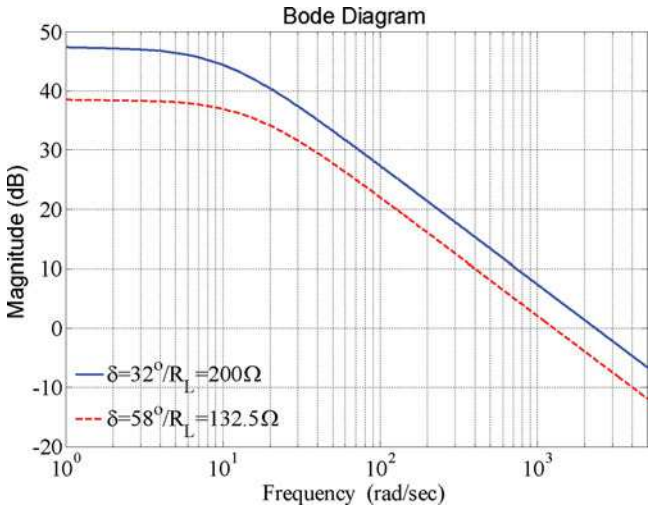

FIGURE 4. Bode magnitude plots for the plant small-signal model reflecting two load conditions.

where $K_0 = \frac{V_{in} R_L}{2\pi f_s L_s N}\left(1 - \frac{2\delta}{\pi}\right)$ and $\tau_0 = R_L C_2$. In Eq. (6), the output voltage is expected to show first-order dynamics in terms of small perturbation on the phase shift.

2.2. Dynamic Analysis

The parameter effect on plant dynamics is illustrated in Table 1, where the parameters are classified as operational parameters and design parameters. In the operating variation, the plant magnitude and time constant change in the same direction as load resistance R_L, while phase shift δ affects DC gain K_0 only. Since the plant dynamics are presented as a first-order transfer function, the value of load resistance affects the system response speed without any impact on the system damping factors, which is different from the non-isolated boost or buck converters. In the design parameters, switching frequency f_s, inductance L_s, and transformer turn ratio N have negative impacts on the plant DC gain. The increasing of the output capacitance slows down the system response through increasing time constant τ_0. These dynamic features are used for the controller synthesis and verified by the experimental tests in Section 4. The small-signal model shows that plant dynamics are not affected by the operating modes of boost, flat-top, and buck.

2.3. Affine Parameterization Procedure

In this section, the affine parameterization design is proposed to synthesize a stable feedback controller to regulate the output voltage. It is also called Q-parameterization or Youla parameterization [27]. The technique has been successfully applied to control the DC/DC buck converter [28], the single-switch quadratic boost converter, and motor drive systems. Different from classical design methods, the affine parameterization starts with the nominal closed-loop transfer function, which stands for the expected closed-loop performance [29]. Since the system model in Eq. (7) is represented by the first-order transfer function, the nominal closed-loop transfer function is correspondingly defined as Eq. (8), which indicates a unit steady-state output [30]:

$$F_Q = \frac{1}{\alpha s + 1}. \tag{8}$$

Ttransfer function $Q(s)$ is derived with the specified closed-loop function F_Q and the inverse transfer function of Eq. (7) as follows:

$$Q(s) = \frac{\tau_0 s + 1}{K_0(\alpha s + 1)}. \tag{9}$$

Controller function $C(s)$ can be parameterized by using Eqs. (7), (8), and (9) as the following standard proportional-integral controller:

$$C(s) = \frac{Q}{1 - F_Q} = K_P + \frac{K_I}{s}, \tag{10}$$

where $K_P = \frac{\tau_0}{K_0 \alpha}$ and $K_I = \frac{1}{K_0 \alpha}$.

δ	R_L (Ω)	Phase margin ϕ_m	Gain margin, G_m
20°	300.0	89.9° at 3.4 kHz	Infinite
32°	200.0	89.9° at 2.8 kHz	Infinite
58°	132.5	90.0° at 1.5 kHz	Infinite

TABLE 4. Phase and gain margins at ideal control conditions.

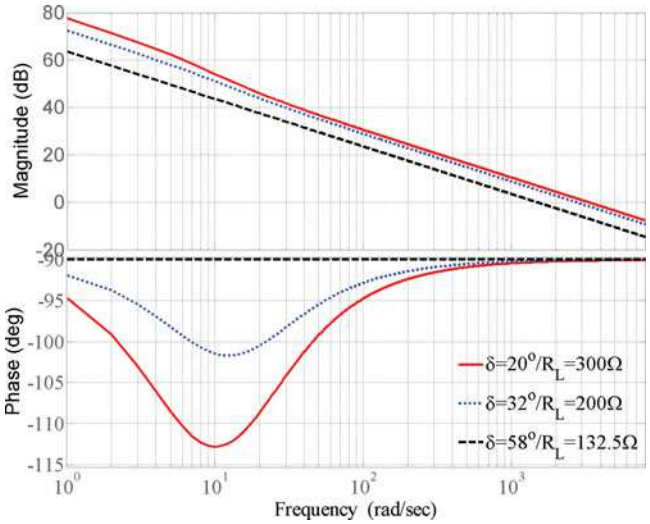

FIGURE 5. Bode plot of $C(s)G_0(s)$ for different load conditions and phase shift degrees.

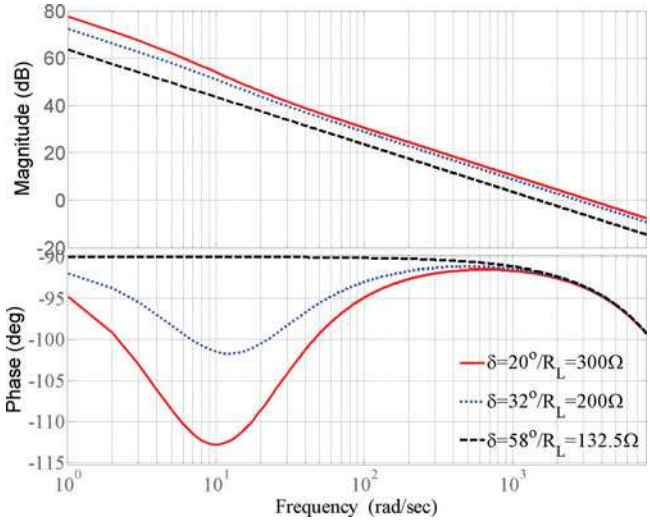

FIGURE 6. Bode plot of $C(s)G_0(s)$ for different load conditions and phase shift degrees with consideration of the time delay.

2.4. Expected Closed-loop Performance

According the design procedure shown above, the coefficient of α should be specified to represent the closed-loop dynamics. For DAB, it is recommended that α be chosen as Eq. (11) to guarantee a faster dynamic response than the original plant but to not suffer too much from measurement noise. The final tuning of α should balance the closed-loop requirement and the practical level of measurement noise:

$$\frac{\tau_0}{10} \leq \alpha \leq \frac{\tau_0}{100}. \tag{11}$$

Since τ_0 varies with the load condition of R_L and the operating condition of δ, determining the constant value of α can be based on the nominal operating condition.

3. CASE STUDY AND ANALYSIS

A DAB prototype is constructed for the case study and design analysis. The system parameters are demonstrated in Table 2, where the rated power of 170 W corresponds to the operating condition of a 58° phase shift, 132.5-Ω load resistance, 150-V output voltage, and 30-V input voltage. The plant transfer functions can be derived by Eq. (7) and are shown in Table 3, which includes the combinations of different values of phase shift δ, load resistance R_L, and corresponding power output P_o, the parameterization results from Eqs. (6) and (7).

δ	R_L (Ω)	Phase margin ϕ_m	Gain margin G_m
20°	300.0	86.0° at 3.3 kHz	23.4 dB at 78.5 kHz
32°	200.0	86.7° at 2.8 kHz	28.3 dB at 78.5 kHz
58°	132.5	88.3° at 1.5 kHz	52.0 dB at 78.5 kHz

TABLE 5. Phase and gain margins considering time delay effect.

3.1. Model Verification

Shown in Figure 3, the mathematical model is verified by comparing the step response with experimental results based on three steady-state conditions when the load resistance is 132.5, 175, and 200 Ω. The small-signal model outputs match well with the dynamics of the experimental test in terms of rising time and setting time. By comparing the measured waveforms, the voltage ripples in Figures 3(b) and 3(c) are higher than that of Figure 3(a). The noisy condition reflects the condition when the load resistance is 175 and 200 Ω. Corresponding to the small-signal analysis shown in Table 1, when the load resistance becomes 200 Ω, the DC gain is 234.4, which is about three times higher than that of 132.5 Ω. The high gain implies the vulnerability to high-frequency noise since the plant frequency bandwidth is also higher, as shown in Figure 4. The zero-crossing frequencies that indicate the cut-off values are 372 and 202 Hz corresponding to 200- and 132.5-Ω load resistances, respectively. The noise phenomena shown in Figure 3 generally correspond to the modeling analyses.

3.2. Controller Synthesis

The rated power level is 170 W, which happens at the condition of phase shift $\delta = 58°$ and load resistance $R_L = 132.5$ Ω. Referring the transfer function shown in Table 3, α is chosen as

$$\alpha = \frac{\tau_0}{100} = 1.50 \times 10^{-3}. \tag{12}$$

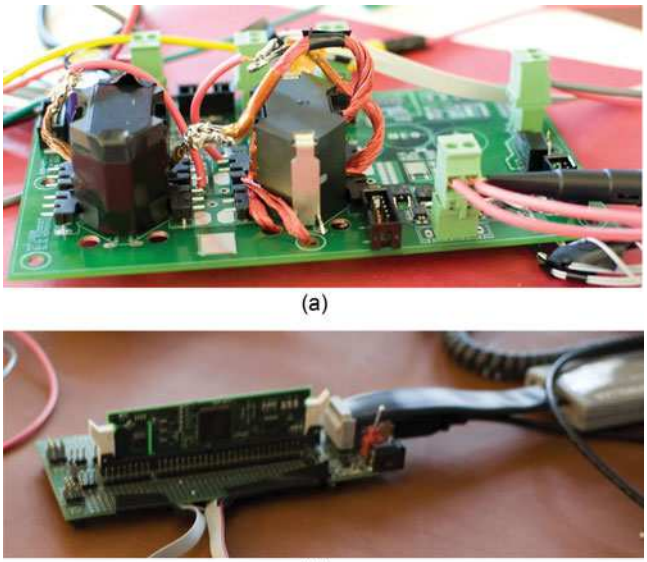

FIGURE 7. Photograph of the DAB control system: (a) power stage and (b) TMS320F2808 microcontroller.

Following the affine parameterization in Eq. (10), the controller transfer function that is based on the rated power condition can be parameterized as

$$C(s) = 1.2 + \frac{17.9}{s}. \tag{13}$$

3.3. Relative Stability Margins

The relative stability margin generally shows the robustness of closed-loop systems under disturbance and model uncertainty. The gain margin is always equal to infinity due the first-order plant model and PI controller. The phase margin is never less than 90°, corresponding to the variation of load resistance R_L and the control variable, as shown in Table 4. The Bode diagram in Figure 5 graphically illustrates the system dynamics in the frequency domain with consideration of the variation of load and phase shifts.

3.4. Digital Redesign

The control algorithm is implemented in a digital controller TMS320F2808, a 32-bit-fixed-point microcontroller from Texas Instruments (Texas, USA). In digital control systems, it is very important to consider the time delay that is caused by sampling and computation. Since the sampling frequency is 100 kHz in the closed loop, a two-sampling time delay is introduced to the system transfer function, which is equal to 20 μs. As a result, the phase and gain margins are recalculated and displayed in Table 5. Even though the phase margin is reduced by several degrees and the gain margin is no longer

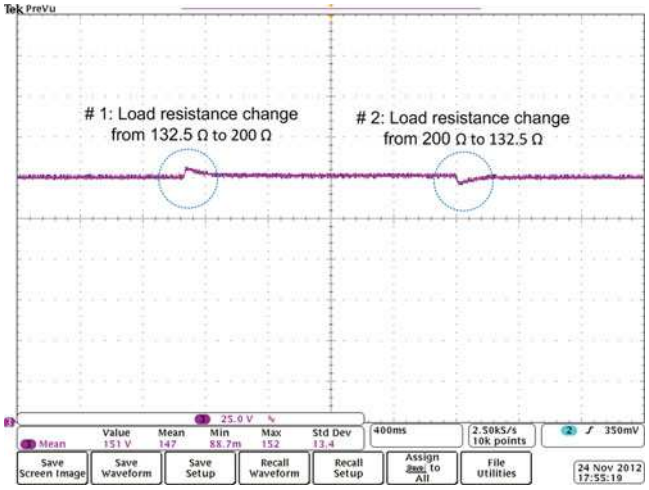

FIGURE 8. Waveform of output voltage disturbed by two-step load changes from 132.5 to 200 Ω and back to 132.5 Ω when the gain scheduling is not applied.

infinity when the time delay is counted by the digital control implementation, the relative stability still keeps very safe margins that guarantee system robustness. The solid closed-loop performance indicates that affine parameterization is an effective tool to synthesize a stable linear controller for DAB applications. The Bode diagram in Figure 6 graphically illustrates the system dynamics in the frequency domain with the consideration of the variation of load and phase operating conditions. By comparing the crossover frequencies at the gain zero-cross points, the Bode diagram shows that the control bandwidth is higher when the steady-state operating condition happens at a low phase shift point, such as 20°. The high control bandwidth implies a good command-following performance and

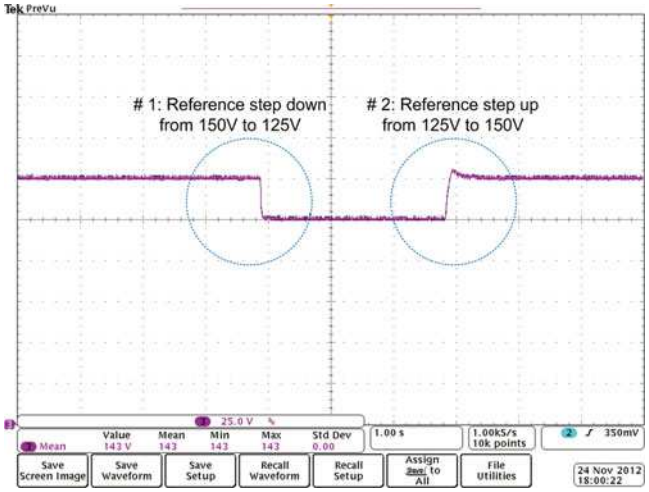

FIGURE 9. Waveform of output voltage following the reference change from 150 to 125 V and back to 150 V.

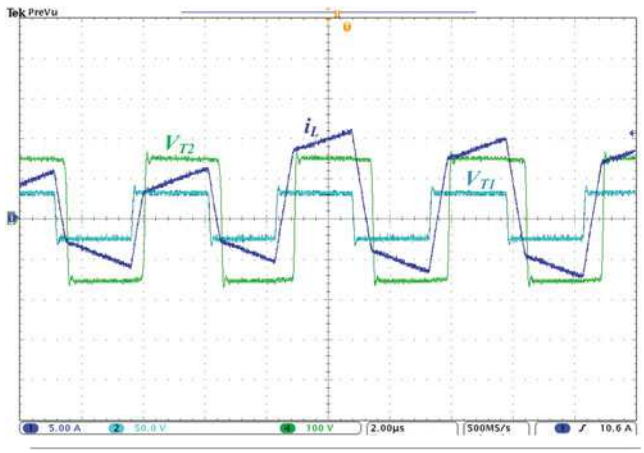

FIGURE 10. Captured transient waveforms of V_{T1} (cyan), V_{T2} (green), and i_L (blue).

effective low-frequency disturbance rejection but vulnerability to high-frequency measurement noise.

4. EXPERIMENTAL EVALUATION

The experimental evaluation includes two aspects: load disturbance rejection and reference command following. The prototype includes the power stage board and the digital signal processor (DSP) control board (see Figure 7), which serve as the power conversion unit and the control unit, respectively. The system specification is shown in Table 2.

4.1. Load Disturbance Rejection

The impact on the output voltage caused by load variation is tested in this section. Figure 8 shows the waveform of the output in response to the load disturbance. The load resistance steps from 132.5 to 200 Ω at moment 1 and changes back to the rated value of 132.5 Ω at moment 2. The voltage is regulated to 150 V against the load disturbance that switches from 132.5 to 200 Ω and back to 132.5 Ω. The over- and under-shoots are less than 2% of the rated voltage. The recovery time is roughly 100 ms.

4.2. Command Following Performance

Figure 9 illustrates the performance test regarding to command following. It shows the waveforms of output voltage following the reference steps changing from 150 to 125 V and back to 150 V. They demonstrate first-order characteristics that agree with the dynamic modeling in Sections 2.1 and 2.2 and closed-loop expectations in Section 3.3. It is noticeable that the step-up setting time is longer than the step-down setting time. When the output voltage enters the steady state of 125 V, the DC gain is 48, which is lower than the value of 84 when the output voltage is 150 V. Thus, the closed-loop response is slower due to the relatively low control bandwidth. The captured waveforms of V_{T1}, V_{T2}, and i_L are demonstrated in Figure 10, which corresponds to the theoretical diagram shown in Figure 2. All symbols shown on the waveforms refer to the definitions illustrated in Figure 1.

5. CONCLUSION

This article presents a systematic and an effective modeling and synthesis approach dealing with voltage regulation issues for designing DAB systems. The first-order characteristics and non-linear features in the DAB are revealed in theory and verified by the experimental tests, which show different perspectives from the conventional DC/DC buck and boost converters. Based on the developed plant model, the controller is designed using the affine parameterization technique, which can be treated as an alternative approach to design linear controllers for stable control loops. The advantage of affine parameterization is that the controller parameters are directly derived from desired closed-loop models. The trade-off decision between system performance and robustness can be clear to the designer.

The closed-loop dynamics and digital control constraints are therefore analyzed in detail. A prototype system is also developed to test the system performance regarding load disturbance rejection and command following. The evaluation proves the effectiveness of the theoretical analysis and proposed methodology to address the key issues in controlling DAB systems. It demonstrates the performance of effective load disturbance rejection and good command following.

ACKNOWLEDGMENTS

The authors would like to thank Dr. David Perreault and the MIT team for valuable support in providing the hardware design reference and technical advice.

FUNDING

This work was funded by the MIT/MI collaboration project. The third author would like to thank support from the National Science Foundation (award 1419076).

REFERENCES

[1] Kheraluwala, M. N., Gascoigne, R. W., Divan, D. M., and Baumann, E. D., "Performance characterization of a high-power dual active bridge," *IEEE Trans. Ind. Appl.*, Vol. 28, No. (6), pp. 1294–1301, 1992.

[2] Oggier, G. G., Garcia, G. O., and Oliva, A. R., "Switching control strategy to minimize dual active bridge converter losses," *IEEE Trans. Power Electron.*, Vol. 24, No. 7, pp. 1826–1838, 2009.

[3] Qin, H., and Kimball, J., "Solid state transformer architecture using AC-AC dual active bridge converter," *IEEE Trans. Ind. Electron.*, Vol. 60, No. 9, pp. 3720–3730, 2012.

[4] Steigerwald, R. L., De Doncker, R. W., and Kheraluwala, M. H., "A comparison of high-power DC-DC soft-switched converter topologies," *IEEE Trans. Ind. Appl.*, Vol. 32, No. 5, pp. 1139–1145, 1996.

[5] Zhao, B., Song, Q., and Liu, W., "Power characterization of isolated bidirectional dual-active-bridge DC-DC converter with dual-phase-shift control," *IEEE Trans. Power Electron.*, Vol. 27, No. 9, pp. 4172–4176, 2012.

[6] Bai, H., and Mi, C., "Eliminate reactive power and increase system efficiency of isolated bidirectional dual-active-bridge DC-DC converters using novel dual-phase-shift control," *IEEE Trans. Power Electron.*, Vol. 23, No. 6, pp. 2905–2914, 2008.

[7] Oggier, G. G., Ledhold, R., Garcia, G. O., Oliva, A. R., Balda, J. C., and Barlow, F., "Extending the ZVS operating range of dual active bridge high-power DC-DC converters," *IEEE Power Electronics Specialists Conference*, pp. 1–7, Jeju, 18–22 June 2006.

[8] Krismer, F., and Kolar, J. W., "Accurate power loss model derivation of a high-current dual active bridge converter for an automotive application," *IEEE Trans. Ind. Electron.*, Vol. 57, No. 3, pp. 881–891, 2010.

[9] Bai, H., Nie, Z., and Mi, C. C., "Experimental comparison of traditional phase-shift, dual-phase-shift, and model-based control of isolated bidirectional DC-DC converters," *IEEE Trans. Power Electron.*, Vol. 25, No. 6, pp. 1444–1449, 2010.

[10] Jain, A. K., and Ayyanar, R., "PWM control of dual active bridge: Comprehensive analysis and experimental verification," *IEEE Trans. Power Electron.*, Vol. 26, No. 4, pp. 1215–1227, 2011.

[11] Krismer, F., and Kolar, J. W., "Efficiency-optimized high-current dual active bridge converter for automotive applications," *IEEE Trans. Ind. Electron.*, Vol. 59, No. 7, pp. 2745–2760, 2012.

[12] Zhou, H., and Khambadkone, A. M., "Hybrid modulation for dual-active-bridge bidirectional converter with extended power range for ultracapacitor application," *IEEE Trans. Ind. Appl.*, Vol. 45, No. 4, pp. 1434–1442, 2009.

[13] Mi, C., Bai, H., Wang, C., and Gargies, S., "Operation, design and control of dual H-bridge-based isolated bidirectional DC-DC converter," *IET Power Electron.*, Vol. 1, No. 4, pp. 507–517, 2008.

[14] Naayagi, R. T., Forsyth, A. J., and Shuttleworth, R., "Bidirectional control of a dual active bridge DC-DC converter for aerospace applications," *IET Power Electron.*, Vol. 5, No. 7, pp. 1104–1118, 2012.

[15] Segaran, D., Holmes, D. G., and McGrath, B. P., "Enhanced load step response for a bidirectional DC-DC converter," *IEEE Trans. Power Electron.*, Vol. 28, No. 1, pp. 371–379, 2013.

[16] Wu, K., de Silva, C. W., and Dunford, W. G., "Stability analysis of isolated bidirectional dual active full-bridge DC-DC converter with triple phase-shift control," *IEEE Trans. Power Electron.*, Vol. 27, No. 4, pp. 2007–2017, 2012.

[17] Xiao, W., Dunford, W. G., Palmer, P. R., and Capel, A., "Regulation of photovoltaic voltage," *IEEE Trans. Ind. Electron.*, Vol. 54, No. 3, pp. 1365–1374, 2007.

[18] Syed, I., and Xiao, W., "Modeling and control of DAB applied in a PV based DC micorgrid," *IEEE International Conference on Power Electronics, Drives and Energy Systems*, pp. 1–6, Bengaluru, 16–19 December 2012.

[19] Zhao, T., Wang, G., Bhattacharya, S., and Huang, A. Q., "Voltage and power balance control for a cascaded H-bridge converter-based solid-state transformer," *IEEE Trans. Power Electron.*, Vol. 28, No. 4, pp. 1523–1532, 2013.

[20] Qin, H., and Kimball, J. W., "Generalized average modeling of dual active bridge DC-DC converter," *IEEE Trans. Power Electron.*, Vol. 27, No. 4, pp. 2078–2084, 2012.

[21] Krismer, F., and Kolar, J. W., "Accurate small-signal model for the digital control of an automotive bidirectional dual active bridge," *IEEE Trans. Power Electron.*, Vol. 24, No. 12, pp. 2756–2768, 2009.

[22] Zhao, C., Round, S. D., and Kolar, J. W., "Full-order averaging modelling of zero-voltage-switching phase-shift bidirectional DC-DC converters," *IET Power Electron.*, Vol. 3, No. 3, pp. 400–410, 2010.

[23] Cardozo, D. D. M., Balda, J. C., Trowler, D., and Mantooth, H. A., "Novel nonlinear control of dual active bridge using simplified converter model," *IEEE Applied Power Electronics Conference and Exposition* (*APEC*), pp. 321–327, Palm Springs, CA, 21–25 February 2010.

[24] Demetriades, G. D., and Nee, H. P., "Dynamic modeling of the dual-active bridge topology for high-power applications," *IEEE Power Electronics Specialists Conference*, pp. 457–464, Rhodes, 15–19 June 2008.

[25] Krishnamurthy, H. K., and Ayyanar, R., "Building block converter module for universal (AC-DC, DC-AC, DC-DC) fully modular power conversion architecture," *IEEE Power Electronics Specialists Conference*, pp. 483–489, Orlando, FL, 17–21 June 2007.

[26] De Doncker, R. W. A. A., Divan, D. M., and Kheraluwala, M. H., "A three-phase soft-switched high-power-density DC/DC converter for high-power applications," *IEEE Trans. Ind. Appl.*, Vol. 27, No. 1, pp. 63–73, 1991.

[27] Youla, D., Bongiorno Jr., J., and Jabr, H., "Modern Wiener–Hopf design of optimal controllers Part I: The single-input-output case," *IEEE Trans. Automat. Control*, Vol. 21, No. 1 pp. 3–13, 1976.

[28] Wei, X., Tsang, K. M., and Chan, W. L., "DC/DC buck converter using internal model control," *Electr. Power Compon. Syst.*, Vol. 37, No. 3, pp. 320–330, 2009.

[29] Goodwin, G. C., Graebe, S. F., and Salgado, M. E., *Control System Design*, Upper Saddle River, NJ: Prentice Hall, Chap. 15, 2001.

[30] Xiao, W., and Zhang, P., "Photovoltaic voltage regulation by affine parameterization," *Int. J. Green Energy*, Vol. 10, No. (3), pp. 302–320, 2013.

BIOGRAPHIES

Imran Syed received his bachelor's degree from National Institute of Technology, Trichy, in 2009. After spending two

years working in the mining industry, he joined Masdar Institute of Science and Technology, where he received his master's degree in electrical power engineering in 2013. He is currently pursuing his Ph.D. at Masdar Institute of Science and Technology, Abu Dhabi, United Arab Emirates. His research interests include power quality devices for microgrid interconnection, solid state transformers, and power system stability improvement.

Weidong Xiao received his master's degree and Ph.D. in electrical engineering from University of British Columbia, Vancouver, Canada, in 2003 and 2007, respectively. He is an associate professor with the department of Electrical Engineering and Computer Science (EECS), Masdar Institute of Science and Technology, Abu Dhabi, United Arab Emirates. In 2010, he was a visiting scholar with the Massachusetts Institute of Technology (MIT), Cambridge, MA, where he worked on the power interfaces for photovoltaic power systems. Prior to his academic career, he worked as an R&D engineering manager with MSR Innovations Inc., Burnaby, Canada, focusing on integration, research, optimization, and design of photovoltaic power systems. He is presently an associate editor of *IEEE Transactions on Industrial Electronics*. His research interest includes photovoltaic power systems, power electronics, dynamic systems and control, and industry applications.

Peng Zhang received his Ph.D. in electrical engineering from University of British Columbia, Vancouver, BC, Canada. He is Assistant Professor of Electrical Engineering at University of Connecticut, Storrs. He was a system planning engineer at British Columbia Hydro and Power Authority (2006–2010), where he planned and designed seven large wind farms. His recent efforts have led to the creation of UCONN's Depot Campus Microgrid and UCONN's first photovoltaic array, a study for hardening northeast utility power infrastructure against extreme weather, and the Building Innovator Award from U.S. DOE. He is a registered professional engineer in British Columbia, Canada, and an editor of *Electric Power Component and Systems*. His research interests include grid integration of renewable energy systems, power system risk assessment, smart grids, microgrids, and smart ocean technologies.